NANO LETTERS
Letter
Cite This: Nano Lett. 2018, 18, 7801−7808
pubs.acs.org/NanoLett

Broadband Achromatic Metasurface-Refractive Optics

Wei Ting Chen,[†] Alexander Y. Zhu,[†] Jared Sisler,[†,‡] Yao-Wei Huang,[†,§] Kerolos M. A. Yousef,[†,∥] Eric Lee,[†,‡] Cheng-Wei Qiu,[§] and Federico Capasso*[,†]

[†]Harvard John A. Paulson School of Engineering and Applied Sciences, Harvard University, Cambridge, Massachusetts 02138, United States

[‡]University of Waterloo, Waterloo ON N2L 3G1, Canada

[§]Department of Electrical and Computer Engineering, National University of Singapore, 117583 Singapore

[∥]College of Biotechnology, Misr University for Science and Technology, Giza, Egypt

S *Supporting Information*

ABSTRACT: Existing methods of correcting for chromatic aberrations in optical systems are limited to two approaches: varying the material dispersion in refractive lenses or incorporating grating dispersion via diffractive optical elements. Recently, single-layer broadband achromatic metasurface lenses have been demonstrated but are limited to diameters on the order of 100 μm due to the large required group delays. Here, we circumvent this limitation and design a metacorrector by combining a tunable phase and artificial dispersion to correct spherical and chromatic aberrations in a large spherical plano-convex lens. The tunability results from a variation in light confinement in sub-wavelength waveguides by locally tailoring the effective refractive index. The effectiveness of this approach is further validated by designing a metacorrector, which greatly increases the bandwidth of a state-of-the-art immersion objective (composed of 14 lenses and 7 types of glasses) from violet to near-infrared wavelengths. This concept of hybrid metasurface-refractive optics combines the advantages of both technologies in terms of size, scalability, complexity, and functionality.

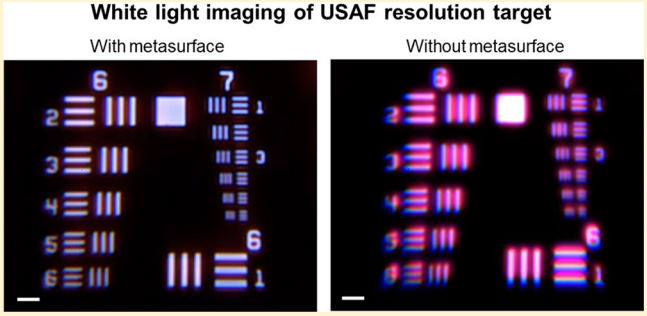

KEYWORDS: *Metasurface, achromatic metalens, dispersion engineering, polarization-insensitive, visible spectrum, titanium dioxide*

Material dispersion is an intrinsic property of all materials in nature. In lens design, it is described by the Abbe number $V = \frac{n_D - 1}{n_F - n_C}$, where n is the refractive index and the subscripts D, F, and C represent wavelengths of 589.3, 486.1, and 656.3 nm, respectively. Although the refractive index difference in the denominator is typically on the order of 0.01, causing a difference in angle of refraction of about 1°, this can lead to significant chromatic aberration in refractive lenses. Since 1730,[1] when cascaded crown and flint glasses were used to compensate for chromatic aberration, the majority of research efforts have focused on developing new glasses with different Abbe numbers. This process is time-consuming, with only about 120 different glasses being available nowadays.[1] More importantly, this approach inevitably leads to bulky composite lenses, which require precise optical alignment. The use of Fresnel lenses in conjunction with refractive lenses is also not ideal. This is because the properties of Fresnel lenses are based on grating dispersion, resulting in a fixed Abbe number of −3.45.[2] This Abbe number is significantly different from that of all refractive lenses (which typically span the range from 20 to 70), resulting in the presence of residual chromatic aberrations in optical system, known as the secondary spectrum.[3] It is therefore very challenging to correct residual aberrations in high-end optical elements by both refractive and diffractive means.

In recent years, metasurfaces, composed of planar arrays of sub-wavelength spaced structures, have been shown to be able to simultaneously manipulate the phase, amplitude, and polarization of light,[4−8] enabling many ultra-compact planar devices, such as polarimeters,[9−11] holograms,[12−14] polarization elements,[15,16] and metalenses.[17−21] Here, we show that the artificial dispersion of a single metasurface can be used to correct spherical and chromatic aberrations of refractive lenses. The dispersion can be fine-tuned across the metasurface by controlling the confinement of light within subwavelength nanostructures, a much more powerful approach than that afforded by refractive and Fresnel optics. As examples, we designed and fabricated a metasurface aberration corrector (hereafter referred to as a metacorrector) that renders a commercial spherical lens achromatic and diffraction-limited across the visible. We show that the resultant metasurface-refractive lens has a much weaker focal length shift compared

Received: September 3, 2018
Revised: November 4, 2018
Published: November 13, 2018

DOI: 10.1021/acs.nanolett.8b03567
Nano Lett. 2018, 18, 7801−7808

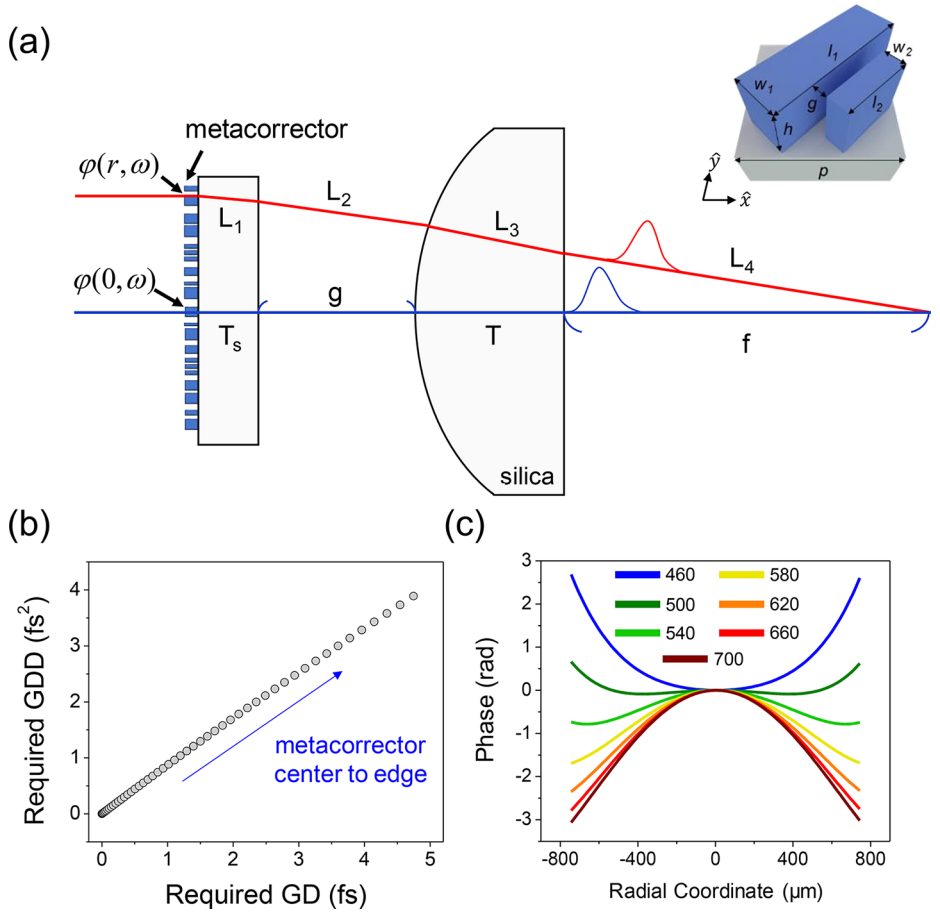

Figure 1. Design of metacorrector. (a) Schematic of a hybrid lens consisting of a metacorrector and a spherical lens to illustrate wavepacket tracing. This drawing is not to scale. The spherical lens is commercially available (LA4249, Thorlabs Inc.). The silica substrate thickness T_s, air gap g, silica lens thickness T, and the parameter f are 0.5, 5, 2.23, and 8.406 mm, respectively. L_1 to L_4 are functions of spatial coordinates and are obtained by the ray-tracing file from Thorlabs Inc. This hybrid lens has a numerical aperture of 0.075. The diameter of the metacorrector is 1.5 mm and is composed of TiO_2 nanofins (inset) with the same height h = 600 nm. Different metalens elements are placed along the x and y directions on the metacorrector with p = 400 nm. (b) Required group delay (GD) and group delay dispersion (GDD) from the center of the metacorrector to its edge. (c) Phase profiles of the metacorrector for different incident wavelengths. The metacorrector has a wavelength-dependent phase profile to correct both spherical and chromatic aberrations.

to refractive and diffractive doublet lenses (Figure S1). To further validate our approach, we also show that a metacorrector can even correct residual aberrations in a Zeiss high-numerical-aperture (NA = 1.45) oil-immersion Fluor microscope objective, which consists of 14 lenses and 7 distinct glass materials, rendering it superachromatic from the violet to the near-infrared.

Although it is possible to realize broadband achromatic transmissive metalenses in the visible spectral regions,[22−24] these metalenses are limited to diameters on the order of 100 μm. Designing a large metalens following these strategies would be very challenging because of limits in achieving the required group delay range across the metalens. For example, to realize a single-layer metalens with a diameter of 1.5 mm and numerical aperture of 0.075, its elements need to provide a group delay difference of 95 fs between light rays traveling through the center and edge of the lens. Based on our previous approach, this would require about 12 μm tall TiO_2 nanostructures (as opposed to 600 nm tall ones in ref 22.). This would correspond to an aspect ratio of about 200, and this number would not be significantly lower by using higher index materials like single-crystal silicon.[25,26] Such a high aspect ratio is well beyond currently available fabrication technologies.

We first explain the design of a metacorrector for a commercially available spherical lens (LA4249, Thorlabs Inc.). Figure 1a shows a schematic diagram of the resulting hybrid lens to illustrate the design principle of wavepacket tracing. A wavepacket, such as the one following the blue trajectory, sequentially passes through the metacorrector, its supporting substrate, an air gap, and, finally, the refractive lens. The metacorrector is designed to possess both a spatially and frequency-dependent phase profile $\varphi(r,\omega)$, such that wavepackets entering at different positions r of the metacorrector can propagate toward the focus and arrive simultaneously with identical temporal profiles compared to the chief wavepacket (the wavepacket passing through the center of the metacorrector). These requirements are to ensure achromatic and diffraction-limited focusing. The group delay $\frac{\partial\varphi(r,\omega)}{\partial\omega}$ and group delay dispersion $\frac{\partial^2\varphi(r,\omega)}{\partial\omega^2}$ provided by the metacorrector control the arrival time and wavepacket width in the time domain, respectively. In practice, one can start from a given angular frequency ω_d and ensure that all wavepackets arrive at

DOI: 10.1021/acs.nanolett.8b03567
Nano Lett. 2018, 18, 7801−7808

the focus in phase for diffraction-limited focusing. This is accomplished by designing the metacorrector to implement the required phase profile given by:

$$\varphi(r,\omega_d) = n\frac{\omega_d}{c}[T_s - L_1(r)] + \frac{\omega_d}{c}[g + f - L_2(r) - L_4(r)] + n\frac{\omega_d}{c}[T - L_3(r)] \quad (3)$$

where n and c are the refractive index of silica and light speed in vacuum, respectively. We set $\varphi(0,\omega_d)$ equal to zero because only the relative phase matters. Note that L_1 to L_4 are functions of radial coordinate r and can be obtained from trigonometric calculations or through commercial ray-tracing software. Here, we obtained these functions at the design wavelength λ_d = 530 nm from the ray-tracing file available on the Thorlabs Web site.[27] Subsequently, to ensure that the wavepackets from the blue and red paths can arrive simultaneously with the same temporal width, the required group delay and group delay dispersion must satisfy the following:

$$\left.\frac{\partial\varphi}{\partial\omega}\right|_{\omega_d} = \frac{n_g}{c}[T_s - L_1(r)] + \frac{1}{c}[g + f - L_2(r) - L_4(r)] + \frac{n_g}{c}[T - L_3(r)] \quad (4)$$

$$\left.\frac{\partial^2\varphi}{\partial\omega^2}\right|_{\omega_d} = \frac{T_s - L_1(r)}{c}\left.\frac{\partial n_g}{\partial\omega}\right|_{\omega_d} + \frac{T - L_3(r)}{c}\left.\frac{\partial n_g}{\partial\omega}\right|_{\omega_d} \quad (5)$$

where f (the distance from the refractive lens to the focus) is independent of frequency, and $n_g = n + \omega\frac{\partial n}{\partial\omega}$ is the group index of silica. Note that c/n_g is the group velocity, which governs the propagation speed of wavepackets; each term in eq 4 can thus be understood to represent the differences in the arrival time of wavepackets, measured with respect to the one traveling along the optical axis. Other higher-order terms can also be obtained in a similar manner. If the glass were dispersionless, eqs 3 and 4 would be equivalent, and the eq 5 would be equal to zero. We emphasize that the role of the metacorrector is to provide group delay and group delay dispersion to compensate for the focal length shift resulting from the finite glass dispersion, i.e., the difference between refractive index and group index. The more dispersive a glass material, the larger the group delay and group delay dispersion required to compensate. However, the difference between group index and refractive index is usually small (about 0.02 for silica at λ = 530 nm); as a result, the corresponding range of group delay required to correct the chromatic aberration of a large refractive lens will be much smaller than what is needed to realize a large diameter achromatic metalens. For a 1.5 mm diameter refractive lens (NA = 0.075), the metacorrector needs to provide a group delay range of 5 fs, while 95 fs is required to realize a metalens of the same diameter and NA.[22] Naturally, the more derivative terms one can include in the design, the better the correction of chromatic aberration that can be achieved. Here, we only consider terms up to the group delay dispersion due to the challenge in designing nanostructures that satisfy eqs 3−5 simultaneously. The required group delay and group delay dispersion from the center to the edge of the metacorrector are shown in Figure 1b. These values, together with the required phase, result in the wavelength-dependent phase profile:

$$\varphi(r,\omega) = \varphi(r,\omega_d) + \left.\frac{\partial\varphi}{\partial\omega}\right|_{\omega=\omega_d}(\omega - \omega_d) + \left.\frac{\partial^2\varphi}{2\partial\omega^2}\right|_{\omega=\omega_d}(\omega - \omega_d)^2 \quad (6)$$

shown in Figure 1c. Note that near λ_d = 530 nm, the phase profile is similar to that of Schmidt plates, which are widely used to correct spherical aberration. At blue wavelengths, because the focal length of the refractive lens becomes shorter, the metacorrector's phase profile behaves like a diverging lens to increase the focal length so that they can be focused at the same position as green wavelengths and vice versa at red wavelengths. Intuitively, the required phase profile $\varphi(r,\omega_d)$ corrects for spherical aberration of the refractive lens and ensures diffraction-limited focusing at λ_d, while the group delay and group delay dispersion minimize chromatic aberration, rendering the whole system achromatic.

Now that the required phase and dispersion (group delay and group delay dispersion) are established, one must consider the non-trivial task of designing (and fabricating) nanostructures that can simultaneously satisfy the required phase, group delay, and group delay dispersion at each coordinate r of the metacorrector for all incident polarizations. We use an element composed of multiple nanofins (see the inset of Figure 1a) to construct the metacorrector. The coupled nanofins support slot waveguide modes that enable us to achieve better dispersion control by changing their widths (w), lengths (l), and gaps (g).[28,29] A scanning electron microscope (SEM) image from a part of the metacorrector is shown in Figure 2a; see Figure S2 for more SEM images. The elements were arranged along ±45° with respect to the x-axis because it enables the metacorrector to correct aberrations for any incident polarization and provides the freedom to control phase in addition to dispersion. This can be understood as

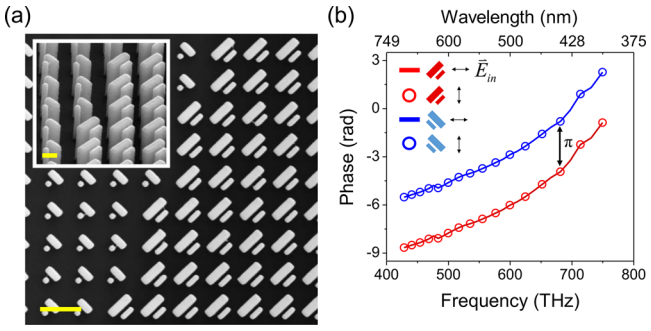

Figure 2. Implementation of metacorrector. (a) Scanning microscope image from a region of the metacorrector, made of TiO_2 nanofins on a glass substrate. Scale bar: 500 nm. The inset shows an oblique view (scale bar: 200 nm). Note that each element is aligned along either 45° or −45°, rendering the phase profile of the metacorrector the same for x and y polarizations. (b) Simulated phase shift of the transmitted electric field, which is orthogonal to the polarization of the incident light (eq 7). The incident polarization is oriented along the x or y axes (depicted by black arrows in the legend). To illustrate the principle, we simulated an element consisting of two nanofins with various rotation angles subjected to illumination with different polarization states. Note that a 90° rotation introduces a π phase shift without changing the dispersion, and the element shows identical phase under x- and y-polarized light rendering the metacorrector capable of correcting aberrations for any incident polarization. The nanofin parameters (w_1, l_1, w_2, l_2, g) equal 90, 420, 70, 200, and 60, respectively, in nanometer units.

DOI: 10.1021/acs.nanolett.8b03567
Nano Lett. 2018, 18, 7801−7808

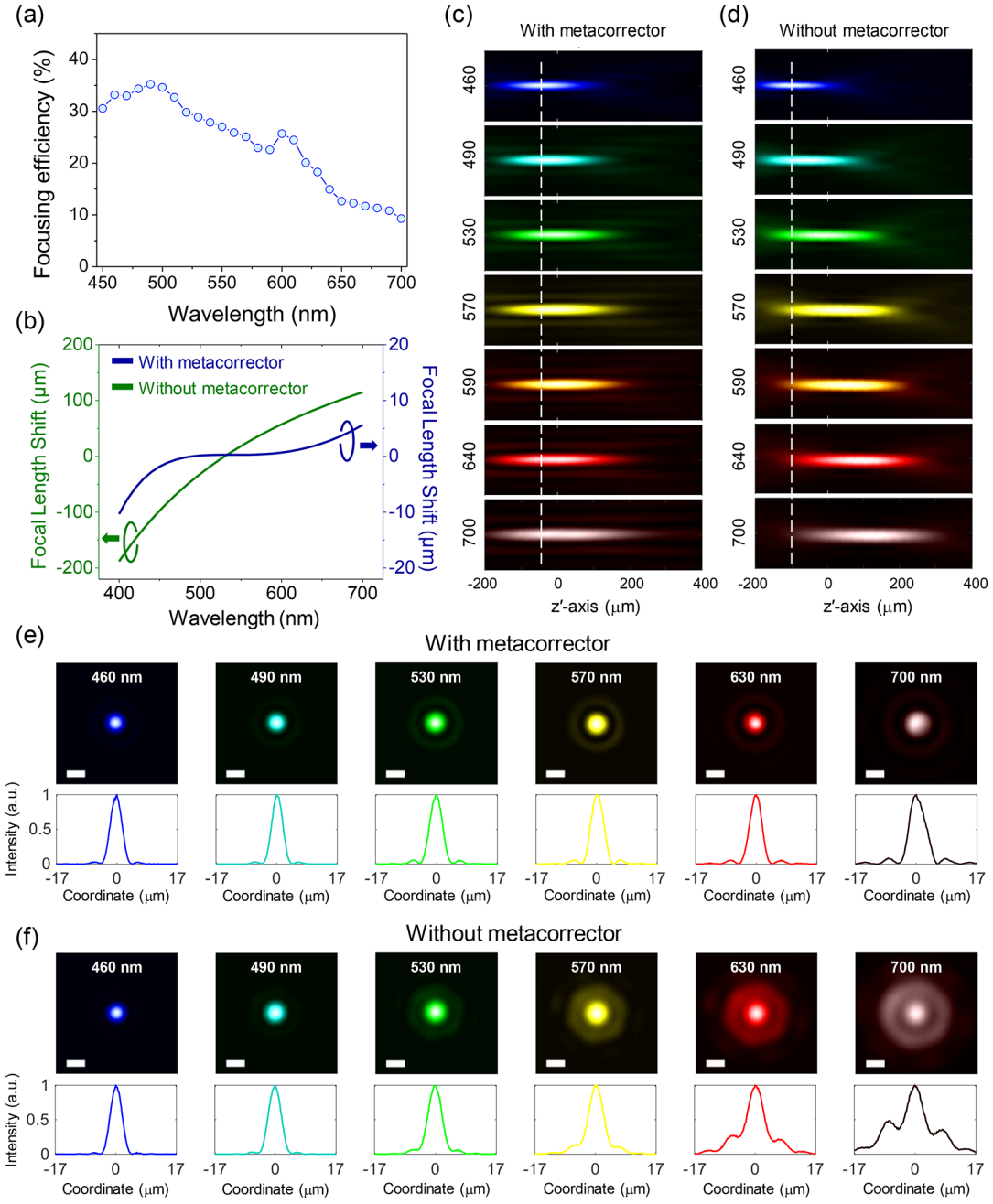

Figure 3. Experimental characterization of the hybrid lens. (a) Efficiency as a function of wavelength. The illumination light source is a tunable broadband laser with a 10 nm bandwidth centered at various wavelengths. The focusing efficiency is defined by the power of focal spot, normalized to the power of incident beam. (b) Simulated focal length shift with (blue) and without (green) the metacorrector. (c, d) Measured intensity distribution in linear scale (in false colors corresponding to their respective wavelengths) for the case (c) with and (d) without the metacorrector. The wavelength of the incident light is labeled on the vertical axis. (e, f) Normalized intensity profiles along the white dashed lines of panels c and d to visualize the effect of chromatic aberration. The wavelengths of the incident laser beam are labeled in white. Scale bar: 5 μm.

follows. When light passes through a nanofin, the transmitted electric field $[E_x^{\text{out}}E_y^{\text{out}}]^T$ can be described by the Jones vector:[30]

$$\begin{bmatrix} E_x^{\text{out}} \\ E_y^{\text{out}} \end{bmatrix} = \frac{\tilde{t}_L + \tilde{t}_S}{2}\begin{bmatrix} 1 & 0 \\ 0 & 1 \end{bmatrix}\begin{bmatrix} E_x^{\text{in}} \\ E_y^{\text{in}} \end{bmatrix} + \frac{\tilde{t}_L - \tilde{t}_S}{2}\begin{bmatrix} \cos(2\alpha) & \sin(2\alpha) \\ \sin(2\alpha) & -\cos(2\alpha) \end{bmatrix}\begin{bmatrix} E_x^{\text{in}} \\ E_y^{\text{in}} \end{bmatrix} \tag{7}$$

where $\tilde{t}_L$ and $\tilde{t}_S$ represent complex transmission coefficients when the electric field of incident light $[E_x^{\text{in}}E_y^{\text{in}}]^T$ is polarized along the long and the short axis of the nanofin, respectively. The symbol T represents the matrix transpose operator and α is the rotation angle of the nanofin in the counterclockwise direction with respect to the x axis. The second term is of primary interest here, and it is designed to impart the designed phase profile $\varphi(r,\omega)$ to the metacorrector. Its two-by-two matrix describes the polarization rotation of the transmitted electric field; it reduces to the Jones matrix of a half-wave plate when the phase difference between $\tilde{t}_L$ and $\tilde{t}_S$ is π. In the case of x-polarized incident light, one can see that a 90° rotation of an element (initially oriented along $\alpha = 45°$) introduces a π-phase shift. This phase shift is frequency-independent, as verified by our simulation results (the red and blue lines of Figure 2b).

DOI: 10.1021/acs.nanolett.8b03567
Nano Lett. 2018, 18, 7801−7808

This characteristic is essential to impart the required phase in addition to the required dispersion. In addition, for a given nanofin aligned along either $\alpha = 45°$ or $-45°$, it can be shown (via the simple matrix algebra of the second term of eq 7) that the output phase under both x- and y-polarized illumination are actually identical. This is confirmed by the simulation results shown by the red circles and lines of Figure 2b. In contrast to previous works,[22,23,31] our metacorrector design is therefore uniquely capable of correcting lens aberrations under any incident polarization, which can be always decomposed in a superposition of x- and y-polarized light. It is worth mentioning that the transmitted light resulting from the second term of eq 7 can have different polarization from the incident beam. However, this will not be a limiting factor for the vast majority of imaging applications where polarization information is not captured.

The implementation of the metacorrector starts from a parameter sweep of the element shown in the inset of Figure 1a to build a library. We used a finite-difference time-domain (FDTD) solver to obtain each element's phase of the y component of electric field as well as the group delay and group delay dispersion under x-polarized illumination (see the Materials and Methods section in the Supporting Information for details). Currently, our library is limited to elements within a range of approximately 5 fs group delay and 10 fs^2 group delay dispersion. The range of these values is important for achieving larger device diameter and numerical aperture and can be increased by engineering their resonant response, stacking multilayers, or increasing the height of the nanofins.[32−36] A particle swarm algorithm was used to choose the element possessing the closest values to the required phase and dispersion given by eqs 3−5 (see Figure S3 for plots of the phase and dispersion of these chosen elements). We fabricated the metacorrector by electron beam lithography followed by atomic layer deposition of TiO_2 and resist removal.[37] The metacorrector was designed with a diameter of 1.5 mm and an air gap g of 5 mm from the refractive lens for ease of experimental measurement. Note that the 5 mm air gap is not crucial; other distances can be used. This final hybrid lens has a numerical aperture NA of 0.075 and an effective focal length of 9.96 mm. Figure 3a plots the focusing efficiency of the hybrid lens as a function of wavelength. It shows a peak focusing efficiency of about 35% (see the Materials and Methods section of the Supporting Information and Figure S4 for measurement details). Efficiencies under different incident polarizations are given in Figure S5. The efficiency is lower than our previous chromatic metalens[38] because, to cover a larger range of group delay, some low-efficiency elements have to be chosen. One possible approach to increase efficiency is by designing each element as a miniature achromatic half-waveplate, which requires additional degrees of freedom not explored in the current design.[39,40] In Figure 3b, we show the simulated focal length shift with and without the metacorrector for comparison. The refractive lens originally exhibits a focal length shift of 300 μm across the visible; with the metacorrector, this value is drastically reduced to about 15 μm. We note that the behavior of the focal length shift is similar to that of conventional triplet lenses. This is a unique feature of the metacorrector-refractive lens that cannot be realized in conventional diffractive-refractive lens design because of a significant secondary spectrum.[41] To better visualize the focal length shift, we also measured the intensity profiles of the focal spot (point spread functions) along the propagation direction z' for different wavelengths in steps of 5 um (Figure 3c,d). By using the metacorrector (Figure 3c), one observes that the chromatic aberration is significantly reduced to only a few tens of micrometers. The measured focal length shift is larger than that of the simulated one (Figure 3b) because of compromises made during the design to simultaneously satisfy the requirements of phase, group delay and group delay dispersion (Figure S3). However, this can be mitigated with a more-exhaustive nanofin parameter search, using methods such as topology optimization.[42,43] Figure 3e,f shows the transverse intensity profiles across a given plane (white dashed lines in panels c and d of Figure 3, respectively). The spherical lens starts showing significant defocusing when the wavelength is larger than 530 nm, while the metacorrector shows focal spots close to diffraction limit from $\lambda = 460$ to 700 nm. Experimental analysis of their focal spot sizes and Strehl ratios can be found in Figure S6. For both cases, the incident beam diameter is fixed to 1.5 mm.

We subsequently used the hybrid lens to image a standard resolution target under incoherent illumination with various bandpass filters (Figure 4a). The spectrum of the light source

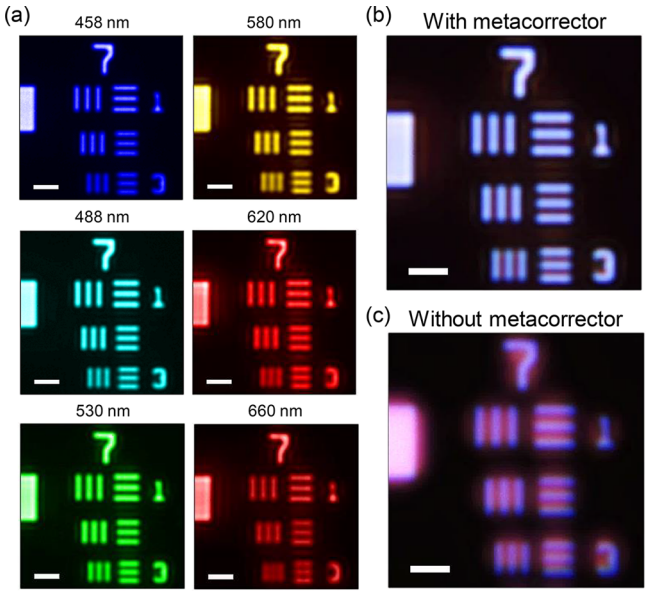

Figure 4. Imaging under incoherent light illumination. (a) Images of a 1951 USAF resolution target formed by the refractive spherical lens with the metacorrector. A few different bandpass filters whose center wavelengths are indicated above each image were used. The line width of the first line in group 7 of the resolution target is 3.91 μm. Scale bars: 15 μm. These images were taken without adjusting the distance between the spherical lens and target. (b, c) A comparison of imaging under white light illumination (b) with and (c) without the metacorrector. These images were taken by a color camera (UI-1540SE, IDS Inc.). The image obtained without the metacorrector shows significant chromatic aberration, resulting in a blurred image. A pair of crossed linear polarizers was used in panels a and b to remove the background.

covers the entire visible wavelength range (Figure S7). The resolution target was brought to focus at a wavelength $\lambda = 460$ nm, and the distance between the target and the hybrid lens was kept constant for all other wavelengths (see the Materials and Methods section in the Supporting Information for measurement details). Note that some patterns cannot be resolved clearly when the wavelength of incidence approaches

DOI: 10.1021/acs.nanolett.8b03567
Nano Lett. 2018, 18, 7801−7808

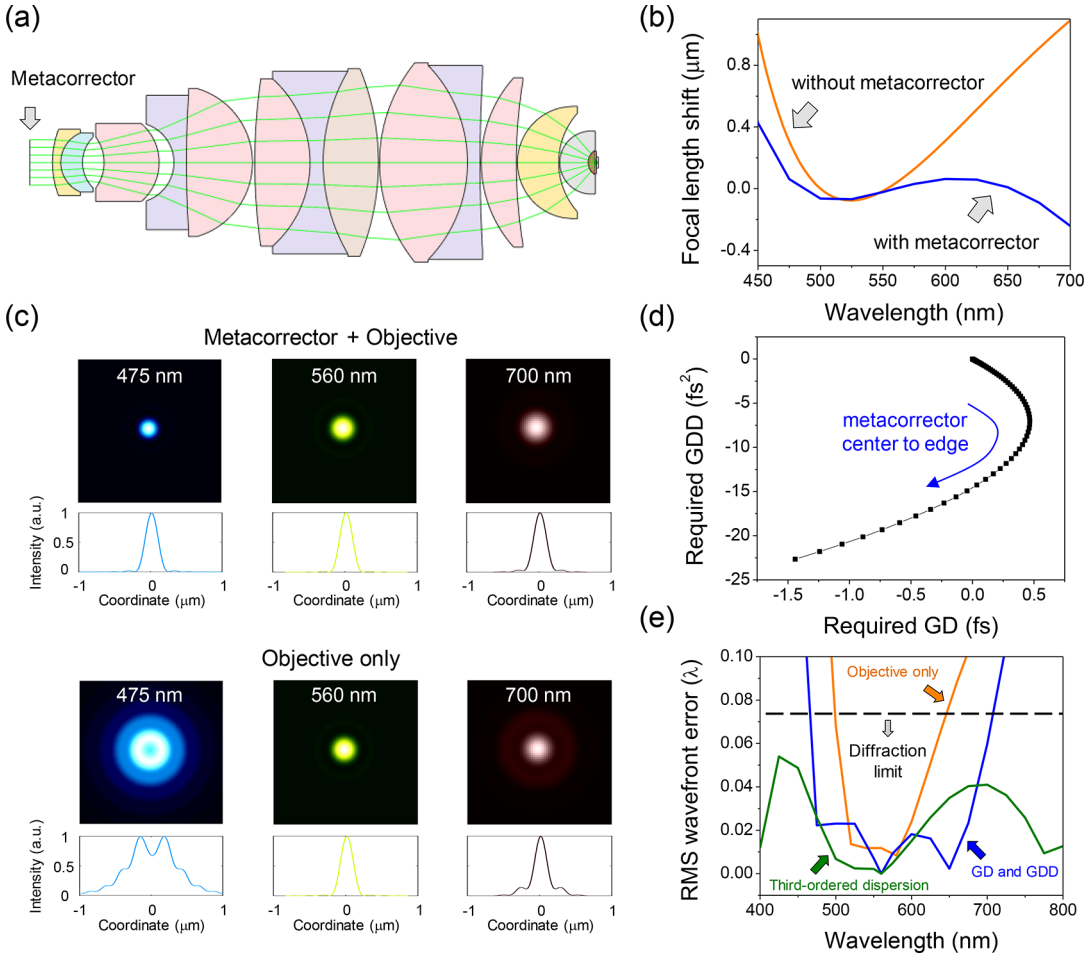

Figure 5. Correcting the aberrations of a Zeiss oil immersion Fluor objective with NA = 1.45. (a) Ray diagram at λ = 560 nm. The metacorrector has a diameter of 4 mm and is placed at the entrance aperture of the objective. The objective consists of 14 lenses made of 7 different glasses (shown by colors). (b) A comparison of simulated focal length shift with and without the metacorrector. (c) Simulated focal spot profiles at three primary wavelengths in the visible for the corrected and non-corrected objective. (d) Required group delay and group delay dispersion from the center of the metacorrector to its edge. (e) Root-mean-square wavefront aberration function for only the objective (orange) and the objective with metacorrector (blue) considering both group delay and group delay dispersion. The objective becomes free of chromatic aberration from violet wavelengths to the near-infrared (green) if one can include the third-order derivative terms $(\frac{\partial^3 \varphi}{\partial \omega^3})$ of the metacorrector to compensate for the high-order dispersion of glasses.

700 nm because their line widths are close to the diffraction-limit of the lens system (NA = 0.075). A comparison using the same experimental setup and procedure for the case without the metacorrector is shown in Figure S8. We also performed white-light imaging of the target, again with and without the metacorrector, shown in Figure 4b,c. Full uncropped images are provided in Figure S9. With the metacorrector, the image shows a clear edge profile whereas, without it, the colors spread apart creating a blurred image and rainbow-like edge, which is characteristic of an imaging system with chromatic aberration.

Finally, to showcase the versatility of our approach, we also designed and simulated a metacorrector for a Zeiss Fluor oil immersion objective with an extremely high NA of 1.45. This Fluor objective possesses the same focal length for only two discrete wavelengths, limiting its operation to a narrow bandwidth. In Figure 5a, we show a ray diagram at λ = 560 nm for the objective with the metacorrector located at its entrance aperture. Data corresponding to each lens of the objective was obtained from a Zeiss patent.[44,45] With the metacorrector, the focal length shift of the objective becomes significantly smaller (see the blue curve in Figure 5b). This leads to diffraction-limited focal spots from λ = 475 to 700 nm; see the first row of Figure 5c. This is in contrast to the case without the metacorrector, as shown in the second row in Figure 5c, where significant defocusing occurs due to the small depth of focus for this extremely high NA objective. In designing the metacorrector for such a system, we only need to cover a range of group delay of ~1.5 fs and group delay dispersion of ~23 fs^2 (see Figure 5d). The required group delay is much smaller than the previous case because the objective has an intrinsically weaker focal length shift compared to the previous Thorlabs lens. Although the required group delay dispersion is higher, it is feasible and still very much within current fabrication capability by introducing a relatively small increase in structure height.[35] Note that adding the metacorrector does not reduce the field of view of the objective, as shown by the plots of off-axis wavefront aberration function in Figure S10. Figure 5e shows a comparison of root-mean-square wavefront aberration function (WAF_{RMS}) in wavelength units for the objective with and without the metacorrector (blue and orange curves, respectively); a WAF_{RMS} value of <0.075λ (Marèchal criterion)

DOI: 10.1021/acs.nanolett.8b03567
Nano Lett. 2018, 18, 7801−7808

is considered to be within the diffraction-limit. If one can design a metacorrector by taking into account up to the third-order derivative ($\frac{\partial^3\varphi(r,\omega)}{\partial\omega^3}$) terms, it is possible to realize a superapochromatic and diffraction-limited high NA objective from the violet to the near-infrared region (green curve of Figure 5e). Such superapochromatic and diffraction-limited focusing in this extremely high NA case is very challenging to realize using natural materials like glasses due to the limited available choice of material dispersion.[46] With our approach of manipulating dispersion in addition to phase, it is feasible to design and experimentally realize a device to improve the performance of this state-of-the-art objective or any other similar optical systems.

To correct other off-axis aberrations, such as coma, field curvature, etc. in addition to chromatic aberration of an imaging system, one can cascade several metasurfaces or pattern two metasurfaces on a substrate. Prior works using the latter approach have shown compact metalenses with large field of view in the visible and infrared.[36,47] Using these methods, one can accumulate larger group delay and group delay dispersion for larger lens diameters and numerical aperture. An alternative approach to correct off-axis aberrations is to engineer the phase profile of the metacorrector as a function of the angle of incidence. This can be achieved by placing dielectric nanostructures on top of a mirror[48,49] or using multilayered dielectric nanostructures.[50]

In conclusion, we have reported metacorrectors that are capable of correcting spherical and chromatic aberrations of any imaging system in a different manner compared to refractive and diffractive optics. These metacorrectors utilize anisotropic nanofins to maintain an accurate phase profile and introduce artificial dispersion for correcting monochromatic and chromatic aberration, respectively. As a proof of concept, we showed that these metacorrectors render a single cost-effective spherical lens achromatic over nearly the entire visible and are even capable of extending the bandwidth of a state-of-the-art NA of 1.45 oil immersion objective significantly, from the violet to the near-infrared. These metasurface aberration correctors can work in tandem with traditional refractive optical components, leading to a major improvement in performance with reduced design complexity and footprint.

■ ASSOCIATED CONTENT

Supporting Information

The Supporting Information is available free of charge on the ACS Publications website at DOI: 10.1021/acs.nanolett.8b03567.

Additional details on materials and methods and figures showing a comparison of chromatic aberration corrections, SEM results, realized phases and dispersions, schematic diagrams, efficiency as a function of polarization, a comparison of focal-spot quality, a spectrum from an incoherent light source, imaging comparisons with and without metacorrectors, broadband incoherent imaging, and root-mean-square wavefront errors (PDF)

■ AUTHOR INFORMATION

Corresponding Author

*E-mail: capasso@seas.harvard.edu.

ORCID

Wei Ting Chen: 0000-0001-8665-9241

Author Contributions

W.T.C. and F.C. conceived the study. A.Y.Z. fabricated the samples. W.T.C., J.S., and E.L. performed simulations and developed codes. W.T.C., A.Y.Z., Y.-W.H., and K.Y. measured the hybrid lens. W.T.C., A.Y.Z., J.S., C.W.Q., and F.C. wrote the manuscript. All authors discussed the results and commented on the manuscript.

Notes

The authors declare no competing financial interest.

■ ACKNOWLEDGMENTS

This work was supported by the Air Force Office of Scientific Research (MURI, grant nos. FA9550-14-1-0389 and FA9550-16-1-0156). This work was performed in part at the Center for Nanoscale Systems (CNS), a member of the National Nanotechnology Coordinated Infrastructure (NNCI), which is supported by the National Science Foundation under NSF award no. 1541959. CNS is part of Harvard University. C.-W.Q. acknowledges financial support from the National Research Foundation, Prime Minister's Office, Singapore under its Competitive Research Program (CRP award no. NRF-CRP15-2015-03). Federico Capasso gratefully acknowledges a gift from Huawei Inc. under its HIRP FLAGSHIP program.

■ REFERENCES

(1) Hartmann, P. *Optical Glass*; SPIE: Bellingham, WA, 2014.

(2) O'Shea, D. C.; Suleski, T. J.; Kathman, A. D.; Prather, D. W. *Diffractive optics: design, fabrication, and test*; SPIE: Bellingham, WA, 2004.

(3) Geary, J. M. *Introduction to Lens Design: With Practical ZEMAX Examples*; Willmann-Bell: Richmond, VA, 2002.

(4) Zheludev, N. I.; Kivshar, Y. S. *Nat. Mater.* **2012**, *11*, 917−924.

(5) Zhan, A.; Colburn, S.; Dodson, C. M.; Majumdar, A. *Sci. Rep.* **2017**, *7*, 1673.

(6) Hsieh, W. T.; Wu, P. C.; Khurgin, J. B.; Tsai, D. P.; Liu, N.; Sun, G. *ACS Photonics* **2018**, *5*, 2541−2548.

(7) Pu, M.; Li, X.; Ma, X.; Wang, Y.; Zhao, Z.; Wang, C.; Hu, C.; Gao, P.; Huang, C.; Ren, H.; Li, X.; Qin, F.; Yang, J.; Gu, M.; Hong, M.; Luo, X. *Sci. Adv.* **2015**, *1*, e1500396.

(8) Khorasaninejad, M.; Capasso, F. *Science* **2017**, *358*, eaam8100.

(9) Chen, W. T.; Török, P.; Foreman, M.; Liao, C. Y.; Tsai, W.-Y.; Wu, P. R.; Tsai, D. P. *Nanotechnology* **2016**, *27*, 224002.

(10) Pors, A.; Nielsen, M. G.; Bozhevolnyi, S. I. *Optica* **2015**, *2*, 716−723.

(11) Rubin, N. A.; Zaidi, A.; Juhl, M.; Li, R. P.; Mueller, J. P. B.; Devlin, R. C.; Leósson, K.; Capasso, F. *Opt. Express* **2018**, *26*, 21455−21478.

(12) Li, X.; Chen, L.; Li, Y.; Zhang, X.; Pu, M.; Zhao, Z.; Ma, X.; Wang, Y.; Hong, M.; Luo, X. *Sci. Adv.* **2016**, *2*, e1601102.

(13) Huang, K.; Dong, Z.; Mei, S.; Zhang, L.; Liu, Y.; Liu, H.; Zhu, H.; Teng, J.; Luk'yanchuk, B.; Yang, K. W. J.; Qiu, C. W. *Laser Photon. Rev.* **2016**, *10*, 500−509.

(14) Zheng, G.; Mühlenbernd, H.; Kenney, M.; Li, G.; Zentgraf, T.; Zhang, S. *Nat. Nanotechnol.* **2015**, *10*, 308−312.

(15) Wu, P. C.; Tsai, W.-Y.; Chen, W. T.; Huang, Y.-W.; Chen, T.-Y.; Chen, J.-W.; Liao, C. Y.; Chu, C. H.; Sun, G.; Tsai, D. P. *Nano Lett.* **2017**, *17*, 445−452.

(16) Lin, D.; Fan, P.; Hasman, E.; Brongersma, M. L. *Science* **2014**, *345*, 298−302.

(17) Arbabi, E.; Arbabi, A.; Kamali, S. M.; Horie, Y.; Faraji-Dana, M.; Faraon, A. *Nat. Commun.* **2018**, *9*, 812.

(18) Li, Y.; Li, X.; Pu, M.; Zhao, Z.; Ma, X.; Wang, Y.; Luo, X. *Sci. Rep.* **2016**, *6*, 19885.

(19) Zhang, L.; Ding, J.; Zheng, H.; An, S.; Lin, H.; Zheng, B.; Du, Q.; Yin, G.; Michon, J.; Zhang, Y.; et al. *Nat. Commun.* **2018**, *9*, 1481.

DOI: 10.1021/acs.nanolett.8b03567
Nano Lett. 2018, 18, 7801−7808

(20) Zhao, Z.; Pu, M.; Gao, H.; Jin, J.; Li, X.; Ma, X.; Wang, Y.; Gao, P.; Luo, X. *Sci. Rep.* **2015**, *5*, 15781.
(21) Li, Z.; Zhang, T.; Wang, Y.; Kong, W.; Zhang, J.; Huang, Y.; Wang, C.; Li, X.; Pu, M.; Luo, X. *Laser Photon. Rev.* **2018**, *12*, 1800064.
(22) Chen, W. T.; Zhu, A. Y.; Sanjeev, V.; Khorasaninejad, M.; Shi, Z.; Lee, E.; Capasso, F. *Nat. Nanotechnol.* **2018**, *13*, 220−226.
(23) Wang, S.; Wu, P. C.; Su, V.-C.; Lai, Y.-C.; Chen, M.-K.; Kuo, H. Y.; Chen, B. H.; Chen, Y. H.; Huang, T.-T.; Wang, J.-H.; Lin, R.-M.; Kuan, C.-H.; Li, T.; Wang, Z.; Zhu, S.; Tsai, D. P. *Nat. Nanotechnol.* **2018**, *13*, 227−232.
(24) Yuan, G. H.; Rogers, E. T. F.; Zheludev, N. I. *Light: Sci. Appl.* **2017**, *6*, e17036.
(25) Sell, D.; Yang, J.; Doshay, S.; Zhang, K.; Fan, J. A. *ACS Photonics* **2016**, *3*, 1919−1925.
(26) Zhou, Z.; Li, J.; Su, R.; Yao, B.; Fang, H.; Li, K.; Zhou, L.; Liu, J.; Stellinga, D.; Reardon, C. P.; et al. *ACS Photonics* **2017**, *4*, 544−551.
(27) *Thorlabs Spherical Singlet Lenses*. https://www.thorlabs.com/thorproduct.cfm?partnumber=LA4249 (accessed August 18, 2018).
(28) Almeida, V. R.; Xu, Q.; Barrios, C. A.; Lipson, M. *Opt. Lett.* **2004**, *29*, 1209−1211.
(29) Tong, L.; Lou, J.; Mazur, E. *Opt. Express* **2004**, *12*, 1025−1035.
(30) Nikolova, L.; Ramanujam, P. S. *Polarization Holography*; Cambridge University Press: Cambridge, U.K., 2009.
(31) Zhang, F.; Zhang, M.; Cai, J.; Ou, Y.; Yu, H. *Appl. Phys. Express* **2018**, *11*, 082004.
(32) Qu, C.; Ma, S.; Hao, J.; Qiu, M.; Li, X.; Xiao, S.; Miao, Z.; Dai, N.; He, Q.; Sun, S.; et al. *Phys. Rev. Lett.* **2015**, *115*, 235503.
(33) Decker, M.; Staude, I.; Falkner, M.; Dominguez, J.; Neshev, D. N.; Brener, I.; Pertsch, T.; Kivshar, Y. S. *Adv. Opt. Mater.* **2015**, *3*, 813−820.
(34) Caloz, C. *Proc. IEEE* **2011**, *99*, 1711−1719.
(35) Shkondin, E.; Takayama, O.; Lindhard, M. J.; Larsen, V. P.; Mar, D. M.; Jensen, F.; Lavrinenko, V. A. *J. Vac. Sci. Technol., A* **2016**, *34*, 031605.
(36) Groever, B.; Chen, W. T.; Capasso, F. *Nano Lett.* **2017**, *17*, 4902−4907.
(37) Devlin, R. C.; Khorasaninejad, M.; Chen, W. T.; Oh, J.; Capasso, F. *Proc. Natl. Acad. Sci. U. S. A.* **2016**, *113*, 10473−10478.
(38) Khorasaninejad, M.; Chen, W. T.; Devlin, R. C.; Oh, J.; Zhu, A. Y.; Capasso, F. *Science* **2016**, *352*, 1190−1194.
(39) Kikuta, H.; Ohira, Y.; Iwata, K. *Appl. Opt.* **1997**, *36*, 1566−1572.
(40) Nordin, G. P.; Deguzman, P. C. *Opt. Express* **1999**, *5*, 163−168.
(41) Stone, T.; George, N. *Appl. Opt.* **1988**, *27*, 2960−2971.
(42) Sell, D.; Yang, J.; Doshay, S.; Yang, R.; Fan, J. A. *Nano Lett.* **2017**, *17*, 3752−3757.
(43) Jensen, J. S.; Sigmund, O. *Laser Photon. Rev.* **2011**, *5*, 308−321.
(44) Kurvits, J. A.; Jiang, M.; Zia, R. *J. Opt. Soc. Am. A* **2015**, *32*, 2082−2092.
(45) Matthae, M.; Schreiber, L.; Faulstich, A.; Kleinschmidt, W. High aperture objective lens. U.S. Patent 6,504,653, Jan. 7, 2003.
(46) Herzberger, M.; McClure, N. R. *Appl. Opt.* **1963**, *2*, 553−560.
(47) Arbabi, A.; Arbabi, E.; Kamali, S. M.; Horie, Y.; Han, S.; Faraon, A. *Nat. Commun.* **2016**, *7*, 13682.
(48) Kamali, S. M.; Arbabi, E.; Arbabi, A.; Horie, Y.; Faraji-Dana, M.; Faraon, A. *Phys. Rev. X* **2017**, *7*, 041056.
(49) Qiu, M.; Jia, M.; Ma, S.; Sun, S.; He, Q.; Zhou, L. *Phys. Rev. Appl.* **2018**, *9*, 054050.
(50) Lin, Z.; Groever, B.; Capasso, F.; Rodriguez, A. W.; Lončar, M. *Phys. Rev. Appl.* **2018**, *9*, 044030.

DOI: 10.1021/acs.nanolett.8b03567
Nano Lett. 2018, 18, 7801−7808